Journal of Institute of Science and Technology, 30(2), 15-23 (2025)
ISSN: 2467-9062 (print), e-ISSN: 2467-9240
https://doi.org/10.3126/jist.v30i2.80204

Research Article

AB INITIO INVESTIGATION OF 1T-$HfTe_2$ MONOLAYER FOR ADSORPTION OF SF_6 DECOMPOSITION GASES

Prabhakar Oli[1,2,3], Bibek Chettri[4], Rajendra Prasad Adhikari[5], Devendra Adhikari[2], Bikash Sharma[6*], Shashit Kumar Yadav[2*]

[1]Central Department of Physics, Tribhuvan University, Kirtipur, Nepal
[2]Department of Physics, Mahendra Morang Adarsh Multiple Campus, Tribhuvan University, Biratnagar, Nepal
[3]Department of Physics, Mechi Multiple Campus, Tribhuvan University, Bhadrapur, Nepal
[4]Department of Physics, Sikkim Manipal Institute of Technology, Sikkim Manipal University, Sikkim, India
[5]Department of Physics, Kathmandu University, Dhulikhel, Kavre, Nepal
[6] Department of Electronics and Communication Engineering, Sikkim Manipal Institute of Technology, Sikkim Manipal University, Sikkim, India
**Correspondence: sashit.yadav@mmamc.tu.edu.np, ju.bikash@gmail.com*

(Received:** June 15, 2025; **Revised:** October 31, 2025; **Accepted:** November 2, 2025**)

ABSTRACT

In this study, the adsorption properties of three byproducts of sulfur hexafluoride (SF_6) decomposition gases on a 1T-$HfTe_2$ monolayer were investigated within the framework of Density Functional Theory (DFT). SF_6 is commonly used in high-voltage transformers as an arc-extinguishing and insulating medium. The Perdew–Burke–Ernzerhof (PBE) functional within the Generalized Gradient Approximation (GGA) was employed for the computational analysis. Adsorption energy (E_{ad}), charge transfer (Q_t), band gap, density of states (DOS), and recovery time (τ) were calculated to understand the adsorption mechanisms of $HfTe_2$ monolayers toward SF_6 decomposition products. The results revealed that the adsorption of SOF_2, SO_2, and SO_2F_2 exhibits chemisorption, with adsorption energies of –0.41, –0.39, and –0.30 eV, respectively. Among these, SOF_2 showed the strongest interaction, while SO_2F_2 exhibited the weakest. The $HfTe_2$ monolayer demonstrated favorable and rapid recovery times, calculated to be 0.14 μs for SOF_2 and 4 μs for SO_2. These findings provide a foundation for the development of 1T-$HfTe_2$-based sensors and adsorbents for use in SF_6-insulated electrical equipment.

Keywords: 1T-$HfTe_2$; DFT; PBE-GGA; Adsorption Properties; Recovery Time; GIS

INTRODUCTION

Sulfur hexafluoride (SF_6) is extensively used as an insulating medium in Gas-Insulated Switchgear (GIS) due to its superior dielectric strength, thermal stability, and arc-quenching capability (Liao *et al.*, 2021; Sarkar *et al.*, 2021; Xin *et al.*, 2001). However, under electrical faults or high-temperature discharges, SF_6 decomposes into toxic and corrosive byproducts such as SO_2, SOF_2, and SO_2F_2 (Sarkar *et al.*, 2021). These gases further react with moisture and oxygen, producing additional secondary species that deteriorate the insulating performance and shorten the operational lifetime of GIS systems (Chettri, *et al.*, 2023). Therefore, early and reliable detection of SF_6 decomposition byproducts is essential for monitoring insulation health and ensuring the safe and continuous operation of GIS equipment.

In recent years, two-dimensional (2D) materials have emerged as highly promising candidates for gas-sensing applications due to their unique structural and electronic characteristics. Their large surface-to-volume ratio, tunable bandgap, and superior carrier mobility enable strong surface interactions and enhanced sensitivity (Khan *et al.*, 2021; Lemme *et al.*, 2014; Mim *et al.*, 2025; Rao *et al.*, 2009; Thayil *et al.*, 2025). While graphene initially attracted attention for its outstanding conductivity, its relatively weak adsorption with gas molecules limits its sensing performance (Uddin *et al.*, 2023). In contrast, transition metal dichalcogenides (TMDs) exhibit buckled structures that facilitate stronger gas adsorption, resulting in high selectivity, rapid response, and improved recovery properties (Chettri *et al.*, 2023; Uddin *et al.*, 2023).

Several TMD-based materials have been explored for gas sensing through both pristine and doped configurations. For instance, metal-decorated MoS_2 exhibited enhanced adsorption strength and sensitivity for CO, NO, and NH_3 gases (Fan *et al.*, 2017). Similarly, Cu-doped HfS_2 demonstrated strong adsorption towards C_2H_4, CH_4, and H_2 gases, highlighting its potential for lithium-ion battery safety monitoring (Li *et al.*, 2024). Pt-doped HfS_2 and $HfSe_2$

have shown selective adsorption of transformer oil and environmental gases such as H_2, C_2H_2, and NO_2 (Cui *et al.*, 2020; Huang *et al.*, 2023), while Pt-doped $HfTe_2$ effectively detected CO and NO_2 depending on the operating temperature (Hu *et al.*, 2022). Other studies on Zr/Hf dichalcogenides confirmed that adsorption can significantly modulate electronic structures, suggesting their tunability for electronic and sensing devices (Raya *et al.*, 2020).

For SF_6 decomposition gas detection, several TMD systems have been investigated. Pt-decorated MoS_2 showed superior adsorption towards SO_2 and SO_2F_2 (Gui *et al.*, 2020). Ni-doped WS_2 exhibited chemisorption for SO_2 and SOF_2 and physisorption for SO_2F_2, indicating selective sensing capabilities (Sarkar *et al.*, 2021). Similarly, SnS_2 monolayers displayed selective adsorption energies of -0.21, -0.17, and -0.15 eV for SO_2, SOF_2, and SO_2F_2, respectively (Guo *et al.*, 2021). Pd-decorated $MoTe_2$ (Li *et al.*, 2024) and Au/Pt/Ag-doped SnS_2 (Wang *et al.*, 2024) have also demonstrated enhanced adsorption and charge transfer, further validating the sensitivity of TMD-based systems toward SF_6 byproducts.

Despite these advancements, most studies rely on metal-doped or defect-engineered TMDs, which may complicate fabrication and reduce long-term stability. In contrast, pristine TMDs with inherent metallic behavior and stable crystal structures could provide efficient, reproducible, and cost-effective sensing platforms. Among them, 1T-$HfTe_2$, a metallic TMD phase, has recently attracted attention for its robust electronic conductivity, stability, and strong orbital hybridization characteristics, features favorable for gas-sensing applications. Therefore, in this work, we systematically investigate the adsorption properties of pristine 1T-$HfTe_2$ toward SF_6 decomposition byproducts (SO_2, SO_2F_2, and SOF_2) using Density Functional Theory (DFT). Key adsorption parameters, including adsorption energy, charge transfer, adsorption distance, and recovery time, are analyzed to assess its sensing potential. The findings reveal that pristine 1T-$HfTe_2$ is a promising candidate for detecting SF_6 byproducts in high-performance GIS systems.

MATERIALS AND METHODS

Computational Details

A $3 \times 3 \times 1$ supercell of $HfTe_2$ was constructed from the unit cell of 1T-$HfTe_2$, which belongs to the space group $P\bar{3}m1$ (Chakraborty & Johari, 2020). All computational investigations were performed using Density Functional Theory (DFT) within the QuantumATK framework (Gritsenko *et al.*, 1995; Smidstrup *et al.*, 2017). The exchange–correlation energy was treated using the Perdew–Burke–Ernzerhof (PBE) functional within the Generalized Gradient Approximation (GGA) (Perdew *et al.*, 1996). For all calculations, Troullier–Martins type norm-conserving pseudopotentials were employed, along with Double-Zeta Polarized (DZP) basis sets (Smidstrup *et al.*, 2017). To accurately describe the interaction between the adsorbed gas molecules and the substrate, van der Waals interactions were accounted for using Grimme's DFT-D2 correction scheme (Grimme *et al.*, 2010). A vacuum layer of 20 Å was applied along the $z-$direction to eliminate spurious interactions between periodic images.

Geometry optimizations were performed until the maximum force on each atom was less than 0.01 eV/Å. The Limited-memory Broyden–Fletcher–Goldfarb–Shanno (LBFGS) algorithm was used for structural relaxation with an energy cutoff of 150 Ha. A $5 \times 5 \times 1$ Monkhorst–Pack $k-$point mesh was employed for Brillouin zone sampling during geometry optimization (Monkhorst & Pack, 1976) with symmetric path M, Γ, K, M. To ensure accurate convergence of the self-consistent field (SCF) cycle, the Pulay mixer algorithm was used with a convergence tolerance of 10^{-5} (Pulay, 1980). For electronic property calculations, a denser $k-$mesh of $10 \times 10 \times 1$ was utilized.

The expression for adsorption energy (E_{ad}) of gas adsorption of $HfTe_2$ can be given as (Karki *et al.*, 2022)

$$E_{ad} = E_{\mathrm{HfTe_2+Gas}} - E_{\mathrm{HfTe_2}} - E_{\mathrm{Gas}} \quad (1)$$

where $E_{\mathrm{HfTe_2}}$ is the energy of pristine $HfTe_2$, $E_{\mathrm{HfTe_2+Gas}}$ is energy of $HfTe_2$ adsorbed with gas and E_{Gas} is the energy of the free gas molecule.

The Mulliken charge transfer (Q_t) of gas adsorption of $HfTe_2$ is calculated using the following relation (Santamaria *et al.*, 1998)

$$Q_t = Q_{adsorbed} - Q_{isolated} \quad (2)$$

where $Q_{adsorbed}$ and $Q_{isolated}$ are the charges carried by gas molecules after and before the adsorption on $HfTe_2$ monolayer.

The recovery time (τ) can be calculated by Vant-Hoffman Arrhenius equation of the form (Ayesh, 2022)

$$\tau = \omega^{-1} e^{-E_{ad}/kT} \quad (3)$$

Herein, ω is the attempt frequency (whose value is taken as 10^{12} s^{-1}) (Ayesh, 2022), k is the Boltzmann constant and T is the room temperature. Moreover, ω represents the vibrational frequency of atoms within the lattice. It is calculated based on Transition State Theory (TST), which explains how chemical reactions

occur by analyzing the energy changes along the reaction pathway. According to TST, a reaction progresses from one stable state (reactants) to another (products) through a reaction coordinate. Both the initial and final states correspond to energy minima, indicating stable configurations, while the pathway between them passes through a maximum energy point known as the transition state or activated complex (Ayesh, 2022; Jacobs *et al.*, 2010).

RESULTS AND DISCUSSION

Tetravalent metals and divalent chalcogens chemically combine to form various phases of transition metal dichalcogenides (TMDs), including 1T, 1T′, 2H, 3R, and T_d. Among these, the 2H phase is the most stable for many TMDs and typically exhibits semiconducting behavior, as observed in materials such as MoS_2, $MoSe_2$, and WS_2. To induce metallic properties, the 2H phase can be transformed into the 1T phase. $HfTe_2$ is one such material that naturally stabilizes in the 1T phase. In this study, the unit cell of 1T-$HfTe_2$ was first optimized using Density Functional Theory (DFT). The optimized lattice parameters were found to be $a = b = 3.99$ Å, $c = 6.69$ Å, the bond length of Hf-Te=2.88 Å and bond angle of Te-Hf-Te= 92.29^0. The obtained values of the work are in good agreement with previously reported values of $a = b = 3.95$ Å (Klipstein *et al.*, 1986), 3.96 Å (Hodul & Stacy, 1985), 4.02 Å (Adam & Bala, 2021) and c =6.67 Å (Klipstein *et al.*, 1986), 6.67 Å (Hodul & Stacy, 1985), 7.63 Å (Adam & Bala, 2021), validating the present computational approach.

As illustrated in Figure 1(a), each Hf atom is coordinated with six Te atoms arranged on either side, forming an octahedral structure, an uncommon configuration in most widely used materials. Figure 1(b) presents the side view of the $3 \times 3 \times 1$ supercell of the $HfTe_2$ monolayer. To further understand the electronic properties of $HfTe_2$, its electronic band structure was calculated and is shown in Figure 1(c). The results indicate that $HfTe_2$ exhibits metallic behavior with a zero bandgap, consistent with previous reports (Klipstein *et al.*, 1986). Both the Conduction Band Minimum (CBM) and the Valence Band Maximum (VBM) are located at the Γ point and overlap above the Fermi level, confirming its metallic nature.

Figure 1(d) shows the density of states (DOS) plot for $HfTe_2$. It can be observed that the density of states below and above the Fermi level touch each other, further supporting its metallic character as indicated by the band structure. Prominent peaks are found at -2.5 eV and -3.5 eV in the valence band, and at 2 eV in the conduction band. Additionally, the CBM is more populated than the VBM at the Fermi level, suggesting the presence of numerous available electronic states, which enhances its conductivity.

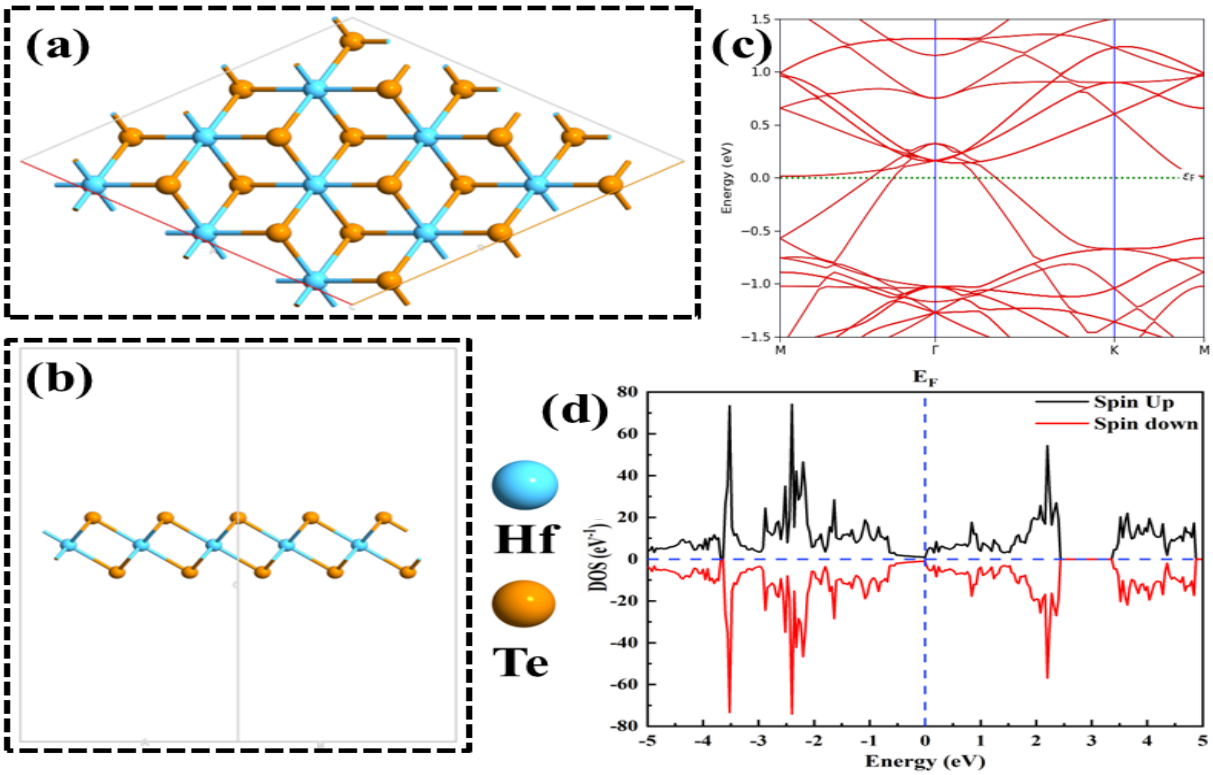

Figure 1. (a) Top view, (b) side view of 1T-$HfTe_2$, (c) band structure, and (d) DOS of the 1T-$HfTe_2$.

Table 1. Adsorption parameters of SF_6 decomposition gases on the top of Hf (Hf^T) and Te (Te^T) atoms of $HfTe_2$ monolayer.

Gas	Adsorption site	Adsorption parameters				
		E_{ad} (eV)	Q_t (e)	D (Å)	E_g (eV)	τ (μs)
SO_2	Hf^T	-0.39387	0.080	2.75	0.00	4.1
	Te^T	-0.31883	0.110	3.08	0.00	-0.32
SO_2F_2	Hf^T	-0.30674	0.004	2.72	0.00	0.14
	Te^T	-0.21100	0.008	3.24	0.00	-0.21
SOF_2	Hf^T	-0.41721	0.046	2.76	0.00	10.1
	Te^T	-0.29558	0.056	3.25	0.00	-0.30

The adsorption properties of three SF_6 decomposition byproducts such as SO_2, SOF_2, and SO_2F_2 on the surface of the 1T-$HfTe_2$ monolayer have been systematically investigated in the work. To accurately identify the preferred adsorption sites for these gases, two initial adsorption positions were considered: at top of Te (Te^T) atom and at the top of Hf (Hf^T) atom, Figure 2. The corresponding adsorption energies (E_{ad}), charge transfers (Q_t), and adsorption distances (D) were calculated using the following relations.

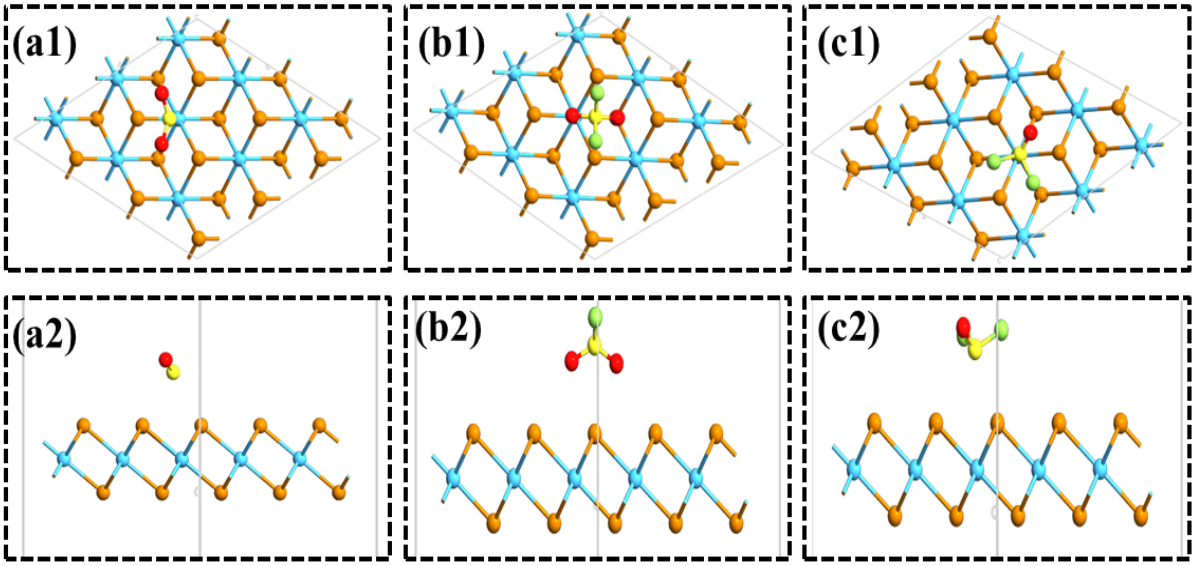

Figure 2. The top and side views of the most stable structures for (a1-a2) SO_2, (b1-b2) SO_2F_2, and (c1-c2) SOF_2 adsorbed on 1T- $HfTe_2$ monolayer.

The calculated adsorption energies for SO_2, SO_2F_2, and SOF_2 at Hf^T site are -0.39378, -0.30674 and -0.41721 eV, respectively which are significantly stronger than those at Te^T site, which are -0.31883, -0.21100 and -0.29558 eV, respectively (Table 1). The negative values of adsorption energy indicate favorable interactions between the gas molecules and the $HfTe_2$ monolayer, characteristic of chemisorption. Since the adsorption energies are more negative at Hf^T, it is considered the energetically favorable site for further analysis. The adsorption energies for SO_2, SOF_2, and SO_2F_2 gases on the surface of a pristine SnS_2 monolayer were calculated to be -0.20, -0.17, and -0.15 eV, respectively (Guo *et al.*, 2021). Subsequently, Wang *et al.* (2024) doped transition metals onto the SnS_2 monolayer to enhance its sensitivity toward these gases. They reported that the adsorption energies for SO_2, SOF_2, and SO_2F_2 on the surface of transition metal-doped SnS_2 were -0.36, -0.25, and -0.15 eV, respectively (Wang *et al.*, 2024). These values are lower in magnitude compared to those obtained in the present work for gas adsorption on the surface of 1T-$HfTe_2$ (Table 1), indicating the superior sensitivity of 1T-$HfTe_2$.

The equilibrium adsorption heights for the most stable configurations are 2.7606 Å for SOF_2, 2.7532 Å for

SO_2, and 2.7201 Å for SO_2F_2, indicating that SOF_2 adsorbs at the greatest distance, while SO_2F_2 is closest to the monolayer surface. The charge transfers from the gas molecules to the $HfTe_2$ surface are 0.046 *e* for SOF_2, 0.080 *e* for SO_2, and 0.004 *e* for SO_2F_2, Table 1. The positive values signify electron transfer from the gas molecules to the $HfTe_2$ monolayer.

Table 2 summarizes the optimized structural parameters of SO_2, SO_2F_2, and SOF_2 molecules before and after adsorption on the surface of the 1T-$HfTe_2$ monolayer. It presents the variations in bond lengths, bond angles, and the shortest adsorption distance between the gas molecules and the $HfTe_2$ substrate. For the SO_2 molecule, the S–O bond length increases slightly from 1.44 Å to 1.48 Å after adsorption, and the O–S–O bond angle changes marginally from 116.61^0 to 117.05^0. In the case of SO_2F_2, the S–O and S–F bond lengths increase from 1.40 Å and 1.55 Å to 1.44 Å and 1.60 Å, respectively, while the bond angles (O–S–O, O–S–F, and F–S–F) show minor deviations. Similarly, for SOF_2, both S–F and S–O bond lengths increase from 1.60 Å and 1.42 Å to 1.67 Å and 1.46 Å, respectively. The O–S–F and F–S–F bond angles slightly increase from 105.16^0 to 105.91^0 and from 92.70^0 to 93.27^0, respectively. The shortest adsorption distances between the gas molecules and the $HfTe_2$ monolayer are approximately 2.88–2.89 Å for all systems, consistent with the findings from Table 1. These subtle geometric changes confirm stable adsorption configurations, which play a crucial role in modulating the electronic properties of the $HfTe_2$-based sensor.

Table 2. Bond length and bond angle before and after the adsorption of SF6 decomposition gases on $HfTe_2$ substrate.

Gas	Before adsorption		After adsorption		$HfTe_2$ bond length (Å)
	Bond length (Å)	Bond angle (in degrees)	Bond length (Å)	Bond angle (in degrees)	
SO_2	S-O=1.44	O-S-O= 116.61	S-O=1.48	O-S-O= 117.05	2.89
SO_2F_2	S-O=1.40	O-S-O=124.65	S-O=1.44	O-S-O=125.30	2.88
	S-F=1.55	O-S-F=108.42	S-F=1.60	O-S-F=107.96	
		F-S-F=96.06		F-S-F=95.42	
SOF_2	O-S=1.42	O-S-F=105.16	O-S=1.46	O-S-F=105.91	2.89
	S-F=1.60	F-S-F=92.70	S-F=1.67	F-S-F=93.27	

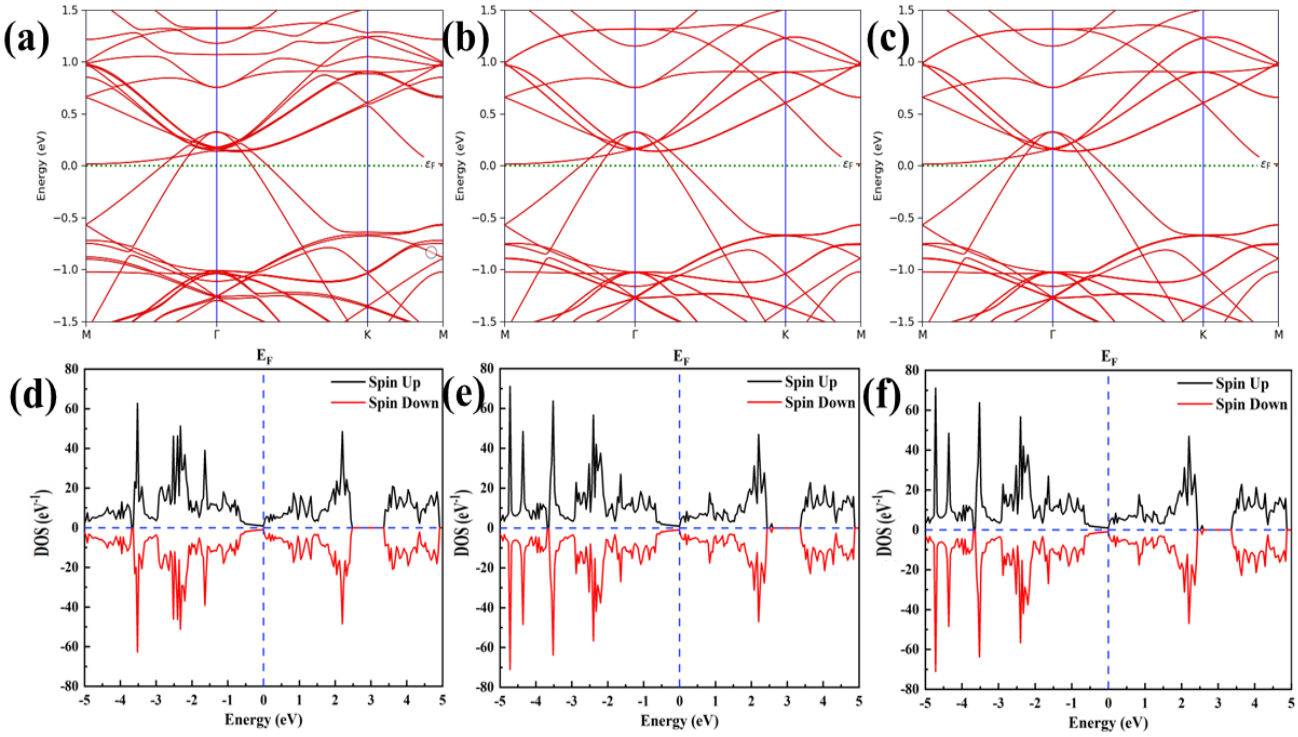

Figure 3. Band structure of (a) SO_2, (b) SO_2F_2, and (c) SOF_2 adsorbed on $HfTe_2$. DOS of (d) SO_2, (e) SO_2F_2, and (f) SOF_2 adsorbed on $HfTe_2$.

To further understand the electronic properties of the $HfTe_2$ monolayer following gas adsorption, the electronic band structure, total density of states (DOS), and partial density of states (PDOS) were calculated and are illustrated in Figures 3(a-f) and 4(a-d). The band structures of all gas-adsorbed systems reveal bands crossing the Fermi level at the Γ symmetry point, indicating a metallic nature, Figure 3(a-c). The band structure and DOS plot for the SO_2 adsorption on $HfTe_2$ closely resembles that of pristine material suggesting minimal impact on the conduction properties, Figure 3(a,d). However, compared to the pristine system, the DOS shows slight changes and more distinct peaks after SO_2 adsorption, indicating charge transfer. The increased density of states near the Fermi level implies improved conductivity relative to the pristine monolayer.

Similarly, Figures 3(b) and 3(e) show the band structure and DOS for the SO_2F_2 adsorption on $HfTe_2$ monolayer. Bands continue to cross the Fermi level at the Γ point, maintaining the metallic character. In the DOS, new sharp peaks appear around 2.5 eV, attributed to gas adsorption effects. Figures 3(c) and 3(f) display the band structure and DOS after SOF_2 adsorption on the material respectively. The system retains its metallic nature, consistent with the other adsorption cases. In the DOS plot, new and prominent peaks emerge at -4.0, -5.0, and around 2.5 eV, irrespective of the pristine $HfTe_2$. Moreover, the Fermi level is noticeably more populated than in the pristine case, confirming the influence of SOF_2 adsorption on the electronic structure. These results demonstrate that gas adsorption induces noticeable changes in the electronic properties of $HfTe_2$, particularly in terms of increased DOS at the Fermi level, which may enhance its performance in sensing applications.

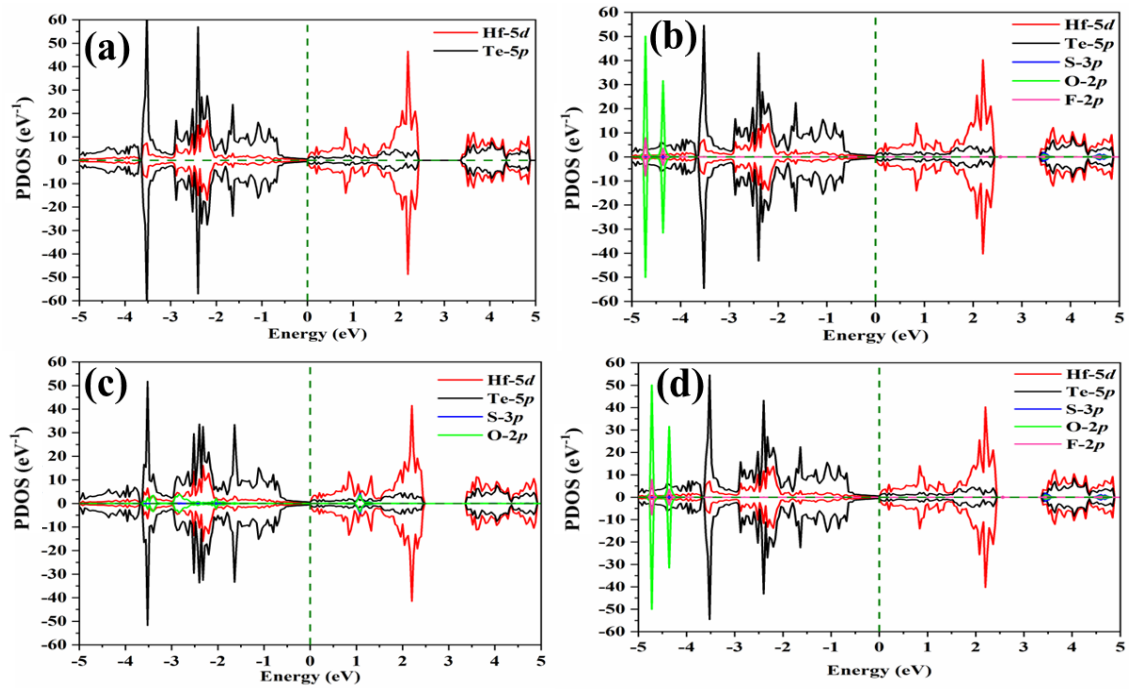

Figure 4. Calculated PDOS of (a) pristine $HfTe_2$, (b) SOF_2 adsorbed $HfTe_2$, (c) SO_2 adsorbed $HfTe_2$, and (d) SO_2F_2 adsorbed $HfTe_2$

To gain deeper insight into the electronic properties, the orbital interactions were examined by computing the partial density of states (PDOS) for pristine $HfTe_2$ and the systems with SO_2, SOF_2, and SO_2F_2 adsorbed on $HfTe_2$. The 5d orbitals of Hf atoms slightly cross the Fermi level, confirming the metallic nature of the pristine $HfTe_2$, Figure 4(a). The Te-5p orbitals dominate the valence band from -1 eV to -4 eV, whereas the Hf-5d orbitals primarily contribute to the conduction band from 0 eV to 2.5 eV. Notable orbital hybridization between Hf-5d and Te-5p orbitals is observed in the energy range of 3.5 eV to 5 eV.

Figure 4(b) displays the PDOS after SOF_2 adsorption on the $HfTe_2$ monolayer. Compared to the pristine case, two new peaks emerge between -4 eV and -5 eV, mainly attributed to O-2p states. Strong orbital hybridization among O-2p, F-2p, and Te-5p orbitals occur around -4.25 eV and -4.75 eV, indicating robust bonding between SOF_2 and the $HfTe_2$ surface. The increased density of states suggests enhanced

electrical conductivity due to gas adsorption. SO_2-adsorbed system shows interaction between O-2p and Hf-5d orbitals in the range of -4 eV to -2 eV, Figure 4(c). Additional hybridization between Hf-5d and Te-5p orbitals occurs between 3.5 eV and 5 eV. Peaks near the valence band maximum (VBM) slightly shift toward the Fermi level, which also contributes to improved conductivity.

Figure 4(d) presents the PDOS for the SO_2F_2 adsorbed on $HfTe_2$ monolayer. Similar to SOF_2, strong orbital hybridization is observed between O-2p, F-2p, and Te-5p orbitals around -4.25 eV and -4.75 eV. This interaction confirms the strong binding between SO_2F_2 and the $HfTe_2$ surface, consistent with the high adsorption energy values. Such strong adsorption may lead to slower recovery dynamics, which is important in practical sensor applications.

For practical gas sensing applications, it is essential that sensors return to their original state promptly after detecting a gas, ensuring readiness for subsequent operations. This attribute is quantified by the recovery time (τ), a critical performance parameter that directly influences the reusability and reliability of the sensor. In this study, the recovery times of SO_2, SOF_2, and SO_2F_2 adsorbed on the $HfTe_2$ monolayer were calculated using Equation (3) and are summarized in Table 1.

The recovery time analysis was conducted at room temperature to evaluate the practical applicability of the sensor under ambient conditions. Among the studied gases, SO_2F_2 exhibited the shortest recovery time of 0.14 μs, indicating a weak interaction with the $HfTe_2$ surface. This quick desorption is advantageous for rapid cycling in real-time sensing environments. Notably, this recovery time is shorter than those reported for metal-modified materials such as SnS_2 *(Hu et al.*, 2022; Raya *et al.*, 2020), highlighting the superior desorption characteristics of pristine $HfTe_2$ for SO_2F_2. In contrast, SOF_2, which forms a stronger chemisorbed bond with the $HfTe_2$ surface, demonstrated a longer recovery time of 10.1 μs, attributed to the enhanced interaction strength and deeper adsorption energy well. The moderate recovery time of 4.1 μs for SO_2 suggests a balance between strong adsorption and acceptable desorption kinetics, making it a promising candidate for selective sensing applications.

These findings confirm that recovery time is inversely related to the adsorption strength. While stronger binding enhances sensitivity, it may also hinder rapid sensor regeneration. Therefore, a trade-off between sensitivity and reusability must be considered in sensor design, and materials like pristine $HfTe_2$ offer a tunable platform to optimize this balance for detecting specific SF_6 decomposition products.

CONCLUSIONS

In this work, the 1T-$HfTe_2$ gas sensor was designed to detect various SF_6 breakdown gases (SOF_2, SO_2, and SO_2F_2). DFT calculations based on first-principles theory were utilized to explore the geometric structure, electronic properties and adsorption properties. Pristine 1T-$HfTe_2$ is a metallic material with zero bandgap**,** making it a suitable candidate for chemiresistive sensing applications due to its high electrical conductivity and tunable surface reactivity. Among the considered SF_6 decomposition gases, SOF_2 exhibits the strongest adsorption with the highest negative adsorption energy and most significant charge transfer, indicating chemisorption and high sensing sensitivity on the Hf site of $HfTe_2$. Adsorption of the target gases causes observable changes in the band structure and density of states (DOS) of $HfTe_2$. The presence of new states and shifts near the Fermi level confirms charge transfer and modulation of electronic properties**,** crucial for resistive sensing. PDOS analysis reveals strong orbital hybridization between O-2p, F-2p, Te-5p, and Hf-5d orbitals**,** especially for SOF_2 and SO_2F_2, supporting the occurrence of robust chemical bonding and electronic interaction between the gas molecules and the monolayer surface.

The calculated recovery times for SO_2F_2 (0.14 μs), SO_2 (4.1 μs), and SOF_2 (10.1 μs) indicate that SO_2F_2 desorbs quickly**;** favoring rapid sensor reusability, while SOF_2 desorption is slower due to stronger adsorption. These values outperform or compete with many metal-decorated 2D materials like SnS_2. Given its strong adsorption capability, tunable electronic response, and relatively fast recovery behavior, pristine 1T-$HfTe_2$ emerges as a promising and efficient sensor material for detecting SF_6 decomposition gases in Gas-Insulated Switchgear systems, aiding in real-time fault diagnosis and condition monitoring.

This work explores the possibility of using an $HfTe_2$ monolayer as a sensing material for SF_6 breakdown leaks during the electric discharge in an insulating gas environment. We anticipate that our calculations can help experimentalists understand the sensing process of $HfTe_2$ monolayers, which will help in its application as a gas sensor in the near future.

ACKNOWLEDGEMENTS

The work was supported by Manipal Research Board (MRB) grants vide: Ref. No. SMU/DoR/2023-274 and Ref. SMU/DoR/2024-71, and DivyaSampark iHUB Roorkee for Devices Materials and Technology

Foundation for the research support vide: Ref. No. 2023/TIH-IITR/590.

AUTHOR CONTRIBUTIONS

Conceptualization: PO, SKY, BS; Investigation: PO, BC, BS, SKY; Methodology: PO, BC, SKY, BS; Data curation: PO, BC; Data analysis: PO, BC, BS, SKY; Writing - original draft: PO; Writing - review and editing: PO, RPA, DA, BS, SKY.

CONFLICT OF INTEREST

The authors declare that they have no known competing financial interests or personal relationships that could have appeared to influence the work reported in this paper.

DATA AVAILABILITY STATEMENT

The data will be made available by the corresponding author upon reasonable request.

REFERENCES

Adam, M. L., & Bala, A. A. (2021). Prediction of phonon-mediated superconductivity and charge density wave in charge doped 1T-$HfTe_2$. *Computational Condensed Matter*, *26*, e00527.

Ayesh, A. I. (2022). H_2S and SO_2 adsorption on Cu doped $MoSe_2$: DFT investigation. *Physics Letters A*, *422*, 127798.

Chakraborty, D., & Johari, P. (2020). First-principles investigation of the 1T-$HfTe_2$ nanosheet for selective gas sensing. *ACS Applied Nano Materials*, *3*(6), 5160–5171.

Chettri, B., Karki, P., Chettri, P., Das, S. K., Kunwar, B., & Sharma, B. (2023). Enhanced adsorption and sensitivity for SF_6 decomposition gas detection on penta $PdSe_2$ monolayer: A Density Functional Theory investigation with van der Waals correction. *Materials Today Communications*, *37*, 107019.

Chettri, B., Karki, P., Chettri, P., Das, S. K., & Sharma, B. (2023). Transition metal dichalcogenides properties, synthesis, and application in nanoelectronics devices. In *Advanced Nanomaterials and Their Applications* (pp. 57–88). CRC Press.

Cui, H., Jia, P., & Peng, X. (2020). Adsorption of SO_2 and NO_2 molecule on intrinsic and Pd-doped $HfSe_2$ monolayer: A first-principles study. *Applied Surface Science*, *513*, 145863.

Fan, Y., Zhang, J., Qiu, Y., Zhu, J., Zhang, Y., & Hu, G. (2017). A DFT study of transition metal (Fe, Co, Ni, Cu, Ag, Au, Rh, Pd, Pt and Ir)-embedded monolayer MoS_2 for gas adsorption. *Computational Materials Science*, *138*, 255–266.

Grimme, S., Antony, J., Ehrlich, S., & Krieg, H. (2010). A consistent and accurate ab initio parametrization of density functional dispersion correction (DFT-D) for the 94 elements H-Pu. *The Journal of Chemical Physics*, *132*(15).

Gritsenko, O., van Leeuwen, R., van Lenthe, E., & Baerends, E. J. (1995). Self-consistent approximation to the Kohn-Sham exchange potential. *Physical Review A*, *51*(3), 1944.

Gui, Y., Shi, J., Yang, P., Li, T., Tang, C., & Xu, L. (2020). Platinum modified MoS_2 monolayer for adsorption and gas sensing of SF_6 decomposition products: A DFT study. *High Voltage*, *5*(4), 454–462.

Guo, S., Hu, X., Huang, Y., Zhou, W., Qu, H., Xu, L., Song, X., Zhang, S., & Zeng, H. (2021). A highly sensitive and selective SnS_2 monolayer sensor in detecting SF_6 decomposition gas. *Applied Surface Science*, *541*, 148494.

Hodul, D. T., & Stacy, A. M. (1985). The effects of nonstoichiometry and electron concentration on the properties of Li_xHfTe_{2-y}. *Journal of Physics and Chemistry of Solids*, *46*(12), 1447–1453.

Hu, J., Zhai, S., Zhang, Q., Cui, H., & Jiang, X. (2022). Two-dimensional $HfTe_2$ monolayer treated by dispersed single Pt atom for hazardous gas Detection: A First-principles study. *Applied Surface Science*, *605*, 154572.

Huang, L., Lu, D., Zeng, W., & Zhou, Q. (2023). Pt-doped HfS_2 monolayer as a novel sensor and scavenger for dissolved gases (H_2, CO_2, CH_4, and C_2H_2) in transformer oil: a density functional theory study. *Langmuir*, *39*(36), 12920–12930.

Jacobs, T. D. B., Gotsmann, B., Lantz, M. A., & Carpick, R. W. (2010). On the application of transition state theory to atomic-scale wear. *Tribology Letters*, *39*(3), 257–271.

Karki, P., Chettri, B., Kunwar, B., & Sharma, B. (2022). A DFT study on sensing performance of H_2S and NO_2 gas molecules on 2D pentagonal $PdSe_2$. *2022 IEEE VLSI Device Circuit and System*, 310–313.

Khan, R., Radoi, A., Rashid, S., Hayat, A., Vasilescu, A., & Andreescu, S. (2021). Two-dimensional nanostructures for electrochemical biosensor. *Sensors*, *21*(10), 3369.

Klipstein, P. C., Guy, D. R. P., Marseglia, E. A., Meakin, J. I., Friend, R. H., & Yoffe, A. D. (1986). Electronic properties of $HfTe_2$. *Journal of Physics C: Solid State Physics*, *19*(25), 4953.

Lemme, M. C., Li, L.-J., Palacios, T., & Schwierz, F. (2014). Two-dimensional materials for electronic applications. *Mrs Bulletin*, *39*(8), 711–718.

Li, X., Zhao, G., Xie, K., Wang, P., Zhang, C., & Lin, L. (2024). Cu-decorated HfS_2 and Cu-embedded HfS_2 for adsorption and gas sensing of lithium-ion

thermal runaway gases: A DFT study. *Surfaces and Interfaces*, *46*, 104028.

Liao, Y., Zhou, Q., Peng, R., & Zeng, W. (2021). Adsorption properties of InP_3 monolayer toward SF_6 decomposed gases: A DFT study. *Physica E: Low-Dimensional Systems and Nanostructures*, *130*, 114689.

Mim, J. J., Rahman, S. M. M., Khan, S., Islam, M. A., Shuvo, R. H., & Hossain, N. (2025). 2D electronic Materials: Integration strategies for electronics and optoelectronics. *Inorganic Chemistry Communications*, 114545.

Monkhorst, H. J., & Pack, J. D. (1976). Special points for Brillouin-zone integrations. *Physical Review B*, *13*(12), 5188.

Perdew, J. P., Burke, K., & Ernzerhof, M. (1996). Generalized gradient approximation made simple. *Physical Review Letters*, *77*(18), 3865.

Pulay, P. (1980). Convergence acceleration of iterative sequences. The case of SCF iteration. *Chemical Physics Letters*, *73*(2), 393–398.

Rao, C. N. R., Sood, A. K., Subrahmanyam, K. S., & Govindaraj, A. (2009). Graphene: the new two-dimensional nanomaterial. *Angewandte Chemie International Edition*, *48*(42), 7752–7777.

Raya, S. S., Ansari, A. S., & Shong, B. (2020). Molecular adsorption of NH_3 and NO_2 on Zr and Hf dichalcogenides (S, Se, Te) monolayers: a density functional theory study. *Nanomaterials*, *10*(6), 1215.

Santamaria, R., Cocho, G., Corona, L., & González, E. (1998). Molecular electrostatic potentials and Mulliken charge populations of DNA mini-sequences. *Chemical Physics*, *227*(3), 317–329.

Sarkar, S., Debnath, P., Chanda, M., & De, D. (2021). DFT Based approach to sense SF_6 decomposed gases (SO_2, SOF_2, SO_2F_2) using Ni doped WS_2 monolayer. *2021 Devices for Integrated Circuit*, 643–647.

Smidstrup, S., Stradi, D., Wellendorff, J., Khomyakov, P. A., Vej-Hansen, U. G., Lee, M.-E., Ghosh, T., Jónsson, E., Jónsson, H., & Stokbro, K. (2017). First-principles Green's-function method for surface calculations: A pseudopotential localized basis set approach. *Physical Review B*, *96*(19), 195309.

Thayil, R., Parne, S. R., & Ramana, C. V. (2025). 2D MoS_2 for next-generation electronics and optoelectronics: from material properties to manufacturing challenges and future prospects. *Small*, *21*(14), 2412467.

Uddin, M. M., Kabir, M. H., Ali, M. A., Hossain, M. M., Khandaker, M. U., Mandal, S., Arifutzzaman, A., & Jana, D. (2023). Graphene-like emerging 2D materials: recent progress, challenges and future outlook. *RSC Advances*, *13*(47), 33336–33375.

Wang, Y., Gui, Y., Yang, J., Jin, G., Yang, P., Gao, M., & Huang, H. (2024). DFT study of metal (Ag, Au, Pt)-modified SnS_2 for adsorption of SF_6 decomposition gases in gas-insulated switchgear. *Langmuir*, *40*(13), 7049–7059.

Xin, L., Junmin, L., Jianyuan, X., & Chenghan, Y. (2001). Numerical calculation of interruption properties of the self-extinguishing type SF_6 circuit breaker during small current interruption. *IEEE Transactions on Magnetics*, *37*(5), 3410–3413.